Effect of varying layouts on the gate temperature for multi-finger AlGaN/GaN HEMTs*

Wang Jianhui(王建辉), Wang Xinhua(王鑫华), Pang Lei(庞磊), Chen Xiaojuan(陈晓娟), Jin Zhi(金智), and Liu Xinyu(刘新宇)†

Key Laboratory of Microwave Devices & Integrated Circuits, Institute of Microelectronics, Chinese Academy of Sciences, Beijing 100029, China

Abstract: The impacts of varying layout geometries on the channel temperature of multi-finger AlGaN/GaN HEMTs are investigated by three-dimensional (3-D) thermal simulations. Micro-Raman thermography is selected to obtain a detailed and accurate temperature distribution of the sample for the verification of the 3-D thermal models. Thermal boundary resistance (TBR) plays an important role in the temperature distribution and is taken into account in the thermal model in order to improve the accuracy of the simulated results. The influence from the number of fingers, finger width and gate pitch on the gate temperature are systematically analysed using 3-D thermal simulations with validated model parameters. Furthermore, a robust method that could efficiently reduce the thermal crosstalk of multi-finger AlGaN/GaN HEMTs is proposed to optimize the thermal design of the device.

Key words: AlGaN/GaN HEMTs; thermal simulation; thermal boundary resistance; thermal management; Raman spectroscopy

DOI: 10.1088/1674-4926/33/9/094004 **PACC:** 6590; 7830

1. Introduction

In the last decade, AlGaN/GaN high electron mobility transistors (HEMTs) have been extensively investigated due to their significant advantages in high-power, high-frequency and high-temperature applications[1]. However, the channel temperature of the device substantially increases to a high level while operating under high power dissipation conditions, commonly known as the self-heating effect, which causes a reduction in device performance and affects the long-term reliability[2]. Compared to single finger AlGaN/GaN HEMTs, devices of multi-finger layout could achieve an exceptionally high output power, but compact designs also aggravate the thermal crosstalk between individual gate fingers and result in a more severe self-heating effect[3]. Therefore, analysis of the influence of varying geometrical layouts in the self-heating phenomenon becomes crucially important for the thermal management of the AlGaN/GaN HEMTs. In addition, the thermal boundary resistances (TBR) between the GaN and substrate layer account for a large portion of the channel temperature, which may cause about a 100 K rise in the vertical temperature distribution of the device[4−6]. Consequently, the TBR effect should be carefully considered in the thermal design of the AlGaN/GaN HEMTs.

Computer aided numerical simulations offer a convenient and economical way to estimate the temperature distribution across various structures of AlGaN/GaN HEMTs. However, in simulation, the computed results probably deviate from the practical realities due to the simplifications and assumptions during the computations. Moreover, thermal parameters of the AlGaN/GaN HEMTs vary significantly in the reported literature[7], which causes serious trouble in the thermal modeling work. Consequently, experimental results are desperately needed to improve the thermal model of the device and validate the accuracy of the simulated results. Several techniques are available to detect the channel temperature of semiconductor devices[8]. Among all the proposed temperature measurement techniques, the micro-Raman thermography method has been proven to be a powerful tool to retrieve the temperature distribution of AlGaN/GaN HEMTs with the advantage of a high spatial resolution, since the heat spot of the device occurs only in a submicron region adjacent to the drain edge of the gate contact[9].

In this work, results of 3-D thermal simulations of the AlGaN/GaN HEMTs with different layouts are compared and discussed. Micro-Raman spectroscopy is utilized to determine the temperature distribution of the sample and its results are used to improve and validate thermal models. Both the TBR at the GaN/substrate interface and the uncertainties of the materials in the thermal parameter are carefully considered for the thermal simulation. Furthermore, a theoretical method that is based on the proposed modeling technique has been developed to decrease the channel temperature of the multi-finger AlGaN/GaN HEMTs.

2. Samples and measurements

The AlGaN/GaN HEMTs with a Ti/Al/Ni/Au drain, source Ohmic contacts and a Ni/Au Schottky gate contact, were fabricated from the epi-structure consisting of 23 nm undoped

* Project supported by the National Basic Research Program of China (No. 2010CB327503) and the National Natural Science Foundation of China (No. 60890191).

† Corresponding author. Email: xyliu@ime.ac.cn

Received 12 February 2012, revised manuscript received 6 April 2012

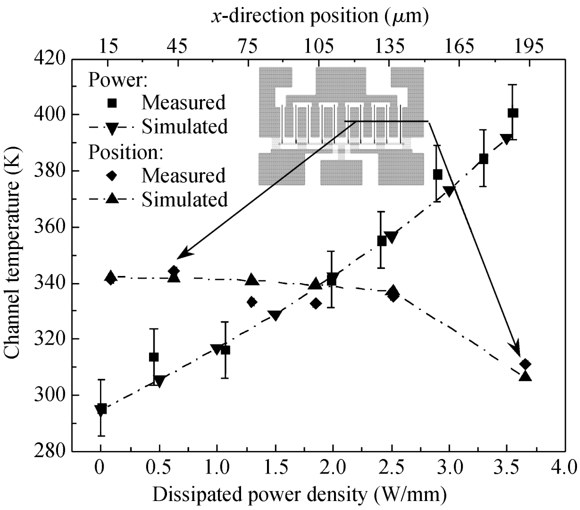

Fig. 1. The measured temperature of the multi-finger AlGaN/GaN HEMTs together with the simulation results.

AlGaN (∼ 26% Al) on a 2 μm intrinsic GaN wafer grown on 400-μm-thick insulating 4H-SiC substrate by low-pressure metal-organic-chemical-vapor deposition (MOCVD) was prepared for measurement. Moreover, the device was passivated by a SiN_x layer of 120 nm. The tested sample composed of 10 fingers of 100 μm gate width, 30 μm gate pitch spacing and a gate length of 200 nm, along with a source–drain gap of 4 μm and a gate-source gap of 1 μm.

Micro-Raman thermography, utilizing the changes in phonon frequency which depends on lattice temperature, was put forward on the aforementioned device to measure the temperature distribution of the AlGaN/GaN HEMTs. Raman spectra were recorded in a backscattering configuration using a confocal micro-Raman spectrometer (HR800) with a spectral resolution of < 0.5 cm^{-1} in the frequency shift range from 450 to 850 cm^{-1}. The 532 nm line of a diode-pumped solid state laser was used as the excitation source with a beam power of 0.1 mW incident on the sample. The spatial resolution of this measurement is about 1 μm, which is comparable to the size of the hot region of the AlGaN/GaN HEMTs. If the measured data is treated with a Lorentz fitting, a Raman shift resolution better than 0.1 cm^{-1} is achieved. The temperature resolution of this measurement is about ±10 K. The device at a drain–source voltage of 0 V was used as a reference to calibrate the relationship between Raman shifts and GaN lattice temperature. E_2 phonon mode is selected to calculate the temperature of the tested device, for the spectral intensity of the E_2 peak is about 10 times higher than A_1(LO), which could greatly increase the signal-to-noise ratio of the measurement. The peak channel temperature of the tested device was acquired versus the increasing power consumption. In addition, the variation of the gate temperature with the finger index is measured under the same power conditions. The results, measured by Raman thermography, are displayed in Fig. 1.

3. Modeling and verification

In the following work, Atlas was chosen as the simulation tool, as it provides general capabilities for physically-based

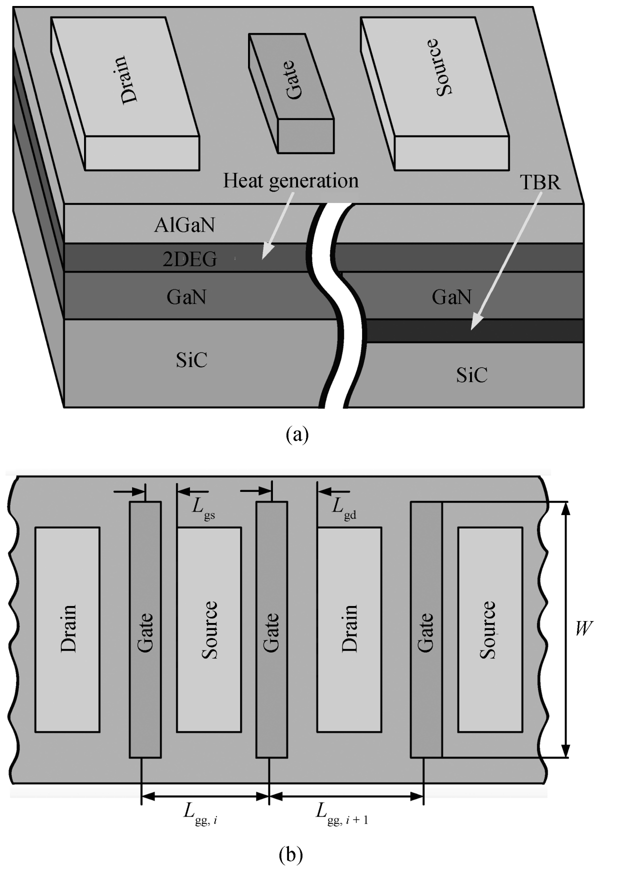

Fig. 2. (a) Schematic diagram of the vertical structure of a realistic device (left) and thermal model (right). (b) Schematic diagram of a typical layout of multi-finger AlGaN/GaN HEMTs. Where L_{gg} is the gate-to-gate pitch, L_{gs} is the gate-to-source spacing and L_{gd} is the gate-to-drain spacing.

two and three-dimensional simulations of semiconductor devices[10]. The exact location of the heat source in the 3-D thermal model is determined by the results of the electro-thermal coupled simulations, which were performed on the corresponding 2-D models. The simulated results manifest that the power of the device during operation is mostly dissipated near the interface between AlGaN and GaN layers and close to the gate edge toward the drain contact with dimensions of about 0.1 × 0.25 μm. Moreover, the effect of TBR on the heat diffusion of AlGaN/GaN HEMTs is carefully considered in the modeling process. The value of TBR was extracted from the temperature discontinuity at the interface between GaN and substrate using the micro-Raman spectroscopy method, which is proposed by Sarua *et al.* The calculated TBR of the material system is about 5.8×10^{-8} m^2K/W, which is less accurate because of the low vertical spatial resolution of the measurement instrument. However, the error of TBR would be compensated in the following modeling step. A 2-μm-thick virtual layer is defined between the GaN and the SiC layers in the thermal model with user-defined thermal conductivity which is calculated from the value of TBR by the method reported by Kuzmik *et al*.[11]. The vertical structure of the thermal model and the test device are shown in Fig. 2(a). Furthermore, Figure 2(b) presents the simplified surface geometries of the multi-finger AlGaN/GaN HEMTs. Actually, the heat dissipates non-uniformly along the

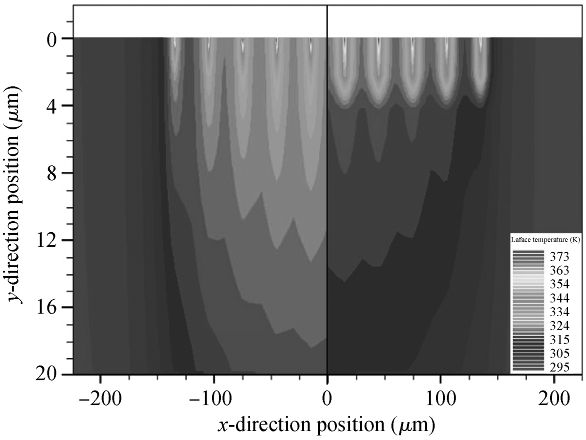

Fig. 3. Temperature distribution of the 10-finger AlGaN/GaN HEMTs (only one half of the device is presented due to the symmetry) calculated from the thermal models with (right) and without (left) TBR taken into consideration.

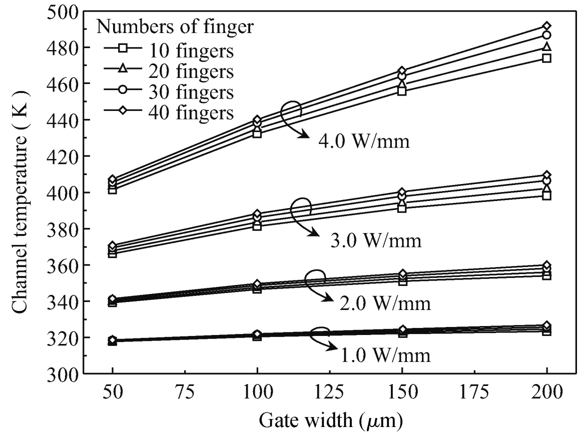

Fig. 4. Peak temperature rise in the central finger of AlGaN/GaN multi-finger HEMTs, with 30-μm-pitch, as a function of gate width.

width of the gate as a result of the temperature variation along the fingers, which may lead to over estimation of the peak temperature[12]. However, with the trends accurately captured, the assumption that the dissipated heat generates a constant heat flux along the width direction is made for simplification. Moreover, the bottom of the substrate in the thermal model is set on the copper heat sink at a constant temperature (295 K), and all the other surfaces are adiabatic.

However, a thermal simulation of AlGaN/GaN HEMTs is a sufficiently challenging task since both of the thermal conductivities and their temperature dependences vary significantly in the reported literature. The heat generated during the operation mainly flows through the GaN and SiC layers to the heatsink. Thus, the thermal conductivities of GaN and SiC are key parameters of the thermal model. However, the influence of the GaN layer on channel temperature is less significant since the GaN layer, compared to SiC's, is really thin. Consequently, the uncertainty of GaN's thermal conductivity slightly affects the accuracy of the simulation results. Therefore, the thermal conductivity of SiC plays a decisive role in the thermal behavior of the model. The temperature gradient in the SiC is generally directed from the GaN layer to the heatsink, which means the adjustment of the thermal conductivity hardly affects the details of the temperature distribution in the active region, which is very important for the thermal optimization of the device. The final value of the SiC's thermal conductivity is determined as a fitting parameter by comparing the simulated results to the measured data. The temperature-dependent thermal conductivities used in the simulations are shown as Eqs. (1)[7] and (2), respectively.

$$\kappa_{\mathrm{GaN}} = 1.0 \times (T/300)^{-0.5}\ \mathrm{W/(cm \cdot K)}, \qquad (1)$$

$$\kappa_{\mathrm{SiC}} = 2.9 \times (T/300)^{-1.35}\ \mathrm{W/(cm \cdot K)}. \qquad (2)$$

The thermal map calculated from the numerical models considering and not considering TBR is demonstrated in Fig. 3, which shows an obvious difference in the temperature distribution. The thermal model that has not considered TBR agrees with the measured data at peak temperatures, but fails to catch the temperature change with the variation of the position of the device. However, the temperature change with gate width (not shown in Fig. 1) and finger index could determine the method for optimizing the device structure. Thus, it's necessary to consider the TBR effect in the thermal model for accurately determining the temperature distribution. Indeed, owing to the idealization of the thermal boundary conditions and the complexity of the device operating mechanisms, there may be subtle differences between the simulated and experimental channel temperature in reality, but since the simulated results agree well with the micro-Raman measurements, the material parameters used could be considered accurate and trustworthy to mold other layout geometries.

4. Simulation and discussion

In multi-finger HEMTs, the thermal interaction between each individual gate causes an additional temperature rise during operation. The maximum temperature, occurring in the center of the device, is treated as the flag temperature to estimate the thermal crosstalk of various structures and geometries. Figure 4 shows a major change in the maximum channel temperature with gate width moving from a 50-μm-width to a 200-μm-width of different finger numbers. There are negligible gate temperature rises with both varied gate width and different gate numbers at low power density. However, owing to an exponential decrease of thermal conductivity and increasingly severe thermal crosstalk, the peak temperature increases very quickly as the power density gets larger. The peak temperature of 200-μm-gate-width devices increased by 18 K (4 W/mm) when the number of gates varied from 10 to 40. Furthermore, the maximum temperature of the device consisting of 40-fingers significantly rises from 407 K to 491 K when the gate width is changed from 50 μm to 200 μm. This comparison demonstrates that the thermal crosstalk is rather sensitive to the finger width.

The influence of gate pitch of multi-finger HEMTs on thermal crosstalk is shown in Fig. 5. As expected, the peak temperatures of the multi-finger AlGaN/GaN HEMTs steadily decrease as the gate-to-gate spacing increases from 20 to 50 μm regardless of the gate width. According to the simulated results, an accelerating temperature rise is found under narrowing

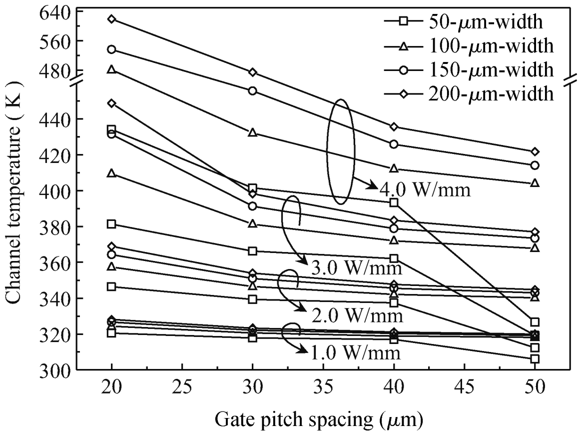

Fig. 5. Peak temperature rise in the central finger of AlGaN/GaN multi-finger HEMTs, consisting of 10 fingers, as a function of gate pitch spacing.

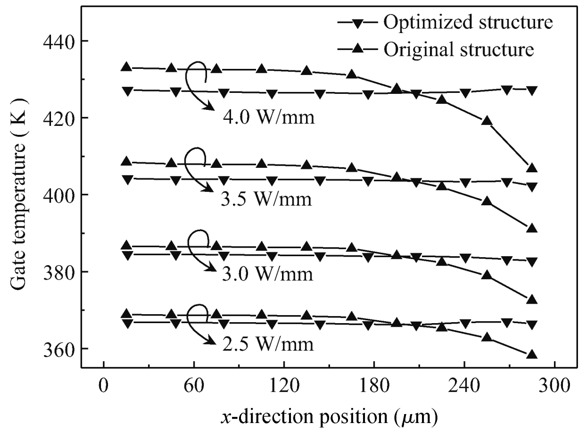

Fig. 6. Gate temperature variation as a function of gate x-composition in 20 fingers AlGaN/GaN HEMTs with 100-μm-width gate.

gate pitch conditions, especially in large gate width devices. The rise of lattice temperature can form a positive feedback with the decrease of the thermal conductivities, which could cause a particularly severe thermal interaction while the gate fingers are moved very close to each other. The simulated results shown in Fig. 5 demonstrate that the peak temperature of more densely packed layouts with 20-μm gate-to-gate spacing is 48 K higher (4 W/mm) than that with 30 μm gate pitch spacing. Finally, it is found that a device layout with enough narrow gate widths could effectively reduce the thermal coupling between the adjacent fingers.

In fact, the gate position of multi-finger HEMTs is always close to the source contact in order to achieve a better electrical performance. Therefore, a deflected gate would cause a slight modulation of the spacing between the neighborhood heat sources, which means the assumption of uniform pitch in the thermal simulation would bring some errors to the results. The realistic gate pitch spacing of the deflected gate design could be calculated as $L_{gg}+(L_{gd}-L_{gs})$ and $L_{gg}-(L_{gd}-L_{gs})$ respectively, and $L_{gd}-L_{gs}$ is commonly less than 3 μm because of the electrical design rules. L_{gd} is the gate to drain spacing and L_{gs} is the gate to source spacing. Simulated results (not shown) reveal that the deflected gate design does not affect the average channel temperature. Moreover, the maximum deviation of the gate temperature is less than 3 K in response to $L_{gd}-L_{gs}$ increasing from 0 to 3 μm. Consequently, the impact of the deflected gate on the temperature distribution is negligible during the thermal investigation.

Gate temperature resulting from a 3-D thermal simulation of 20-finger AlGaN/GaN HEMTs with uniform gate spacing is shown in Fig. 6 (only one half of the device is presented due to symmetry). Channel temperature of uniform pitch device is relatively high in the center fingers and decreases towards the two sides of the outer fingers. In addition, the simulated results manifest that the decrease of channel temperature is merely through several outer fingers, while the inner gate temperature of the device appears fairly uniform for a wide range of gate widths and numbers. This phenomenon is explained as the thermal diffusion from the heat source takes effect in a limited distance, thus crosstalk between the two far enough gate fingers is neglectable. Moreover, especially for large devices, the heat generated during the operation is primarily conducted into the substrate perpendicular to the heatsink and results in uniform gate temperature of the inner fingers.

Obviously, a uniform gate temperature would bring additional benefits for the cooling design and long-term reliability. Thus, gate pitch spacing treated as a function of gate number index for optimizing the thermal behavior of multi-finger HEMTs is shown in Fig. 2(b). In the following discussions, only one half of the problem is considered due to the symmetry of the thermal model. All of the gates are divided exactly into two groups according to the profile of the channel temperature and different optimization strategies are used for each part. For the inner part, the gate temperature is almost equal to each other. Consequently, the gate-to-gate spacing of the inner part between neighborhood gates is simply given by

$$L_{gg,\,inner}=\frac{(n_1-0.5)\,L_{gg0}+L_{op}}{n_1-0.5}, \quad (3)$$

where L_{gg0} is the gate spacing of original uniform pitch device, n_1 is the gate number in the inner group and L_{op} is a variable parameter for optimizing the gate-to-gate spacing.

The gate pitch spacing of outer parts between the gate i and gate $i+1$ is given by[13]

$$L_{gg,\,outer,\,i}=L_{gg,\,inner}+a\left(4i^3+3i^2+i\right), \quad (4)$$

where i is the gate finger index and varies from 0 to n_2-1. n_2 is the gate number in the outer part. Note that the gate pitch of the outer group is equal to $L_{gg,\,inner}$ with the finger index at 0. The reality width for optimization of outer gate spacing can be calculated as

$$W_{outer}=n_2L_{gg0}-0.5L_{gg,\,inner}-L_{op}. \quad (5)$$

The optimized results of 20-finger AlGaN/GaN HEMTs are given in Fig. 6 as an example, which shows that broad uniformity of the gate temperature is achieved in the optimized structure. The optimum value for the parameter n_1, n_2, L_{op} and a are 6, 4, 11 and −0.23. Comparison between the optimized and original design indicates that the peak temperature of the device substantially drops from 433 to 427 K at a power density of 4 W/mm. Furthermore, as a means of creating more uniform temperature distributions from finger to finger, the optimization method is reasonably robust with respect to changes in the operating power densities. Finally, further simulations reveal that the optimization method is also effective regardless of layout variations in finger number and gate width as long as the parameters are properly selected.

5. Conclusions

In summary, 3-D thermal simulations using a novel modeling method are performed to investigate the influence of various layout designs on the gate temperature of multi-finger AlGaN/GaN HEMTs. Micro-Raman measurements are utilized to eliminate the uncertainties of thermal parameters and validate the accuracy of the thermal model. Moreover, TBR at the GaN/SiC interface is carefully considered in the simulation for investigating the thermal interaction of the multi-finger device. Furthermore, the impacts of numbers of gate, gate width and gate spacing on the channel temperature of the multi-finger device are methodically analyzed and the simulation results indicate that both the gate width and pitch spacing are critical factors in the thermal design. Finally, an efficient optimization method for layout design that roughly decreases the peak channel temperature by 6 K in the example is suggested.

Acknowledgement

The authors would like to acknowledge Liu Yulong at Institute of Physics of Chinese Academy of Sciences for his contributions during the micro-Raman experiment.

References

[1] Mishra U K, Parikh P, Wu Y F. AlGaN/GaN HEMTs—an overview of device operation and applications. Proc IEEE, 2002, 90(6): 1022

[2] Gaska R, Osinsky A, Yang J W, et al. Self-heating in high-power AlGaN-GaN HFETs. IEEE Electron Device Lett, 1998, 19(3) :89

[3] Kuball M, Rajasingam S, Sarua A, et al. Measurement of temperature distribution in multifinger AlGaN/GaN heterostructure field-effect transistors using micro-Raman spectroscopy. Appl Phys Lett, 2003, 82(1): 124

[4] Sarua A, Ji H, Hilton K P, et al. Thermal boundary resistance between GaN and substrate in AlGaN/GaN electronic devices. IEEE Trans Electron Devices, 2007, 54(12): 3152

[5] Riedel G J, Pomeroy J W, Hilton K P, et al. Reducing thermal resistance of AlGaN/GaN electronic devices using novel nucleation layers. IEEE Electron Device Lett, 2009, 30(2): 103

[6] Kuzmik J, Bychikhin S, Pogany D, et al. Investigation of the thermal boundary resistance at the III-nitride/substrate interface using optical methods. J Appl Phys, 2007, 101: 054508

[7] Cappelluti F, Furno M, Angelini A, et al. On the substrate thermal optimization in SiC-based backside-mounted high-power GaN FETs. IEEE Trans Electron Devices, 2007, 54(7): 1744

[8] Blackburn D L. Temperature measurements of semiconductor devices–a review. Twentieth Annual IEEE Semiconductor Thermal Measurement and Management Symposium, 2004: 70

[9] Killat N, Kuball M, Chou T, et al. Temperature assessment of AlGaN/GaN HEMTs: a comparative study by Raman, electrical and IR thermography. IEEE International Reliability Physics Symposium, 2010: 528

[10] www.silvaco.com

[11] Kuzmik J, Bychikhin S, Neuburger M, et al. Transient thermal characterization of AlGaN/GaN HEMTs grown on silicon. IEEE Trans Electron Devices, 2005, 52(8): 1698

[12] Heller E R, Crespo A. Electro-thermal modeling of multifinger AlGaN/GaN HEMT device operation including thermal substrate effects. Microelectron Reliab, 2008, 48: 45

[13] Garven M, Calame J P. Simulation and optimization of gate temperatures in GaN-on-SiC monolithic microwave integrated circuits. IEEE Trans Compon Packag Technol, 2009, 32(1): 63